DMD Fast Forward. Published on March 16, 2023 as DOI: 10.1124/dmd.122.001113
This article has not been copyedited and formatted. The final version may differ from this version.

Characterization of Enzymes Involved in Nintedanib Metabolism in Humans

Shimon Nakashima[1]*, Rei Sato[1]*, Tatsuki Fukami[1,2], Takashi Kudo[3], Shiori Hashiba[1], Gaku Morinaga[3], Masataka Nakano[1,2], Eva Ludwig-Schwellinger[4], Akiko Matsui[3], Naoki Ishiguro[3], Thomas Ebner[4], and Miki Nakajima[1,2]

[1]Drug Metabolism and Toxicology, Faculty of Pharmaceutical Sciences, and

[2]WPI Nano Life Science Institute (WPI-NanoLSI), Kanazawa University, Kanazawa, Japan

[3]Department of Pharmacokinetics and Nonclinical Safety, Nippon Boehringer Ingelheim Co., Ltd., Hyogo, Japan

[4]Department of Drug Metabolism and Pharmacokinetics, Boehringer Ingelheim Pharma GmbH & Co KG, Biberach, Germany

*These authors equally contributed to this work.

DMD Fast Forward. Published on March 16, 2023 as DOI: 10.1124/dmd.122.001113
This article has not been copyedited and formatted. The final version may differ from this version.

Running title: Metabolic enzymes in nintedanib metabolism

To whom all correspondence should be sent:

Miki Nakajima, Ph.D.

Drug Metabolism and Toxicology

Faculty of Pharmaceutical Sciences

Kanazawa University

Kakuma-machi, Kanazawa 920-1192, Japan

E-mail: nmiki@p.kanazawa-u.ac.jp

Number of text pages: 29

Number of tables: 4

Number of figures: 7

Number of references: 51

Number of words in abstract: 250 words

Number of words in introduction: 603 words

Number of words in discussion: 1,277 words

Abbreviations

AADAC, Arylacetamide deacetylase; ABHD10, α/β Hydrolase domain containing 10; APEH, Acylamino peptide hydrolase; BNPP, Bis (*p*-nitrophenyl) phosphate; CES, Carboxylesterase; DFP, Diisopropyl fluorophosphate; DMSO, Dimethyl sulfoxide; EGCg, Epigallocatechin gallate; GI, gastronintestinal tract; HLC, Human liver cytosol; HLM, Human liver microsomes; HLH, Human liver homogenate; PMSF, Phenylmethylsulfonyl fluoride; PON, Paraoxonase; SA, D-Saccharic acid 1,4-lactone monohydrate; S9, Supernatant 9,000*g*

DMD Fast Forward. Published on March 16, 2023 as DOI: 10.1124/dmd.122.001113
This article has not been copyedited and formatted. The final version may differ from this version.

Abstract

Nintedanib, which is used to treat idiopathic pulmonary fibrosis and non-small cell lung cancer, is metabolized to a pharmacologically inactive carboxylate derivative, BIBF1202, via hydrolysis and subsequently by glucuronidation to BIBF1202 acyl-glucuronide (BIBF1202-G). Since BIBF1202-G contains an ester bond, it can be hydrolytically cleaved to BIBF1202. In this study, we sought to characterize these metabolic reactions in the human liver and intestine. Nintedanib hydrolysis was detected in human liver microsomes (HLM) (CL_{int}: 102.8 ± 18.9 μL/min/mg protein) but not in small intestinal preparations. CES1 was suggested to be responsible for nintedanib hydrolysis according to experiments using recombinant hydrolases and hydrolase inhibitors as well as proteomic correlation analysis using 25 individual HLM. BIBF1202 glucuronidation in HLM (3.6 ± 0.3 μL/min/mg protein) was higher than that in human intestinal microsomes (1.5 ± 0.06 μL/min/mg protein). UGT1A1 and gastrointestinal UGT1A7, UGT1A8, and UGT1A10 were able to mediate BIBF1202 glucuronidation. The impact of UGT1A1 on glucuronidation was supported by the finding that liver microsomes from subjects homozygous for the *UGT1A1*28* allele showed significantly lower activity than those from subjects carrying the wild-type *UGT1A1* allele. Interestingly, BIBF1202-G was converted to BIBF1202 in HLS9 at 70-fold higher rates than the rates of BIBF1202 glucuronidation. An inhibition study and proteomic correlation analysis suggested that β-glucuronidase is responsible for hepatic BIBF1202-G deglucuronidation. In conclusion, the major metabolic reactions of nintedanib in the human liver and intestine were quantitatively and thoroughly elucidated. This information could be helpful to understand the inter- and intraindividual variability in the efficacy of nintedanib.

Keywords: Nintedanib, hydrolysis, CES1, UGT1A1, deglucuronidation

DMD Fast Forward. Published on March 16, 2023 as DOI: 10.1124/dmd.122.001113
This article has not been copyedited and formatted. The final version may differ from this version.

Significance Statement

To our knowledge, this is the first study to characterize the enzymes responsible for each step of nintedanib metabolism in the human body. We found that β-glucuronidase may contribute to BIBF1202-G deglucuronidation.

DMD Fast Forward. Published on March 16, 2023 as DOI: 10.1124/dmd.122.001113
This article has not been copyedited and formatted. The final version may differ from this version.

Introduction

Idiopathic pulmonary fibrosis (IPF) is a prototype of chronic, progressive, and fibrotic lethal lung disease of unknown cause; IPF is a debilitating lifetime-limiting condition with a median survival ranging from 2.5 to 3.5 years (Richeldi et al., 2017; Raghu et al., 2015). Nintedanib, which inhibits vascular endothelial growth factor receptor, platelet-derived growth factor receptor, and fibroblast growth factor receptor, is used for the treatment of IPF. In addition, nintedanib is also used in various countries for the treatment of non-small cell lung cancer. Although its therapeutic efficacy has been proven, several adverse events, including diarrhea and hepatic dysfunction, the mechanisms of which have not been elucidated, have been reported in some cases (Azuma et al., 2016).

Metabolism is the major pathway of nintedanib clearance. The predominant nintedanib metabolic pathways are hydrolysis to the pharmacologically inactive carboxylate derivative BIBF1202 and subsequent glucuronidation to BIBF1202 acyl-glucuronide (BIBF1202-G) (Stopfer et al., 2011). After oral administration of 200 mg nintedanib to cancer patients, the dose-normalized $AUC_{0\text{-}12}$ values of nintedanib, BIBF1202, and BIBF1202-G were 0.819, 1.08, and 1.64 (ng/mL·h)/mg, respectively (FDA Center for Drug Evaluation and Research, 2014). Nintedanib, BIBF1202, and BIBF1202-G are excreted in feces at concentrations of 19.9%, 58.4%, and 0.1% of the initial dose within 72 h after oral administration, respectively (Wind et al., 2019). The data suggest that BIBF1202-G is likely deglucuronidated to BIBF1202 in the gut. Overall, it was reported that nintedanib undergoes rapid and extensive first-pass metabolism (Wind et al., 2019).

Several hydrolases are involved in drug metabolism, viz. carboxylesterase (CES) 1, CES2, and arylacetamide deacetylase (AADAC), and have been well characterized (Fukami et al., 2022). CES1 tends to target compounds with relatively large acyl groups, whereas CES2 and AADAC tend to target compounds with relatively small acyl groups (Fukami et al., 2015). Therefore, the hydrolysis of nintedanib is expected to be catalyzed by CES1 given the large size of its acyl group, but the responsible enzyme remains to be identified. Paraoxonase

DMD Fast Forward. Published on March 16, 2023 as DOI: 10.1124/dmd.122.001113
This article has not been copyedited and formatted. The final version may differ from this version.

(PON) isoforms (PON1, PON2, and PON3), which are expressed not only in the liver but also in the plasma, are also able to hydrolyze some drugs, including pilocarpine and simvastatin (Hioki et al., 2011, Draganov et al., 2005). Whether nintedanib is hydrolyzed by PON isoforms in plasma has not been investigated.

For subsequent metabolism, i.e., glucuronidation, Wind et al. (2019) reported that UGT1A1, UGT1A7, UGT1A8, and UGT1A10 catalyze the formation of BIBF1202-G from BIBF1202. UGT1A1 is expressed in the liver and small intestine, whereas UGT1A7, UGT1A8, and UGT1A10 are expressed in the intestine but not in the liver. It is unknown whether the liver or intestine shows higher metabolic clearance with respect to BIBF1202 glucuronidation. Although glucuronidation is generally recognized as a detoxification process, the glucuronidation of compounds with a carboxylic acid to acyl-glucuronides is considered to be associated with overt toxicity in some cases. This toxicity occurs because some acyl-glucuronides are chemically unstable and reactive and can covalently bind to cellular proteins (Bailey et al., 2003). Interestingly, acyl-glucuronides can be converted to corresponding carboxylic compounds by not only gut flora but also enzymes expressed in human tissues. For example, it is known that acyl-glucuronides of valproic acid and mycophenolic acid are hydrolyzed to corresponding carboxylic compounds by acylpeptide hydrolase (APEH) (Suzuki et al., 2010) and α/β hydrolase domain containing 10 (ABHD10) (Iwamura et al., 2012) in the human liver, respectively. However, it remains to be elucidated whether BIBF1202-G is hydrolyzed to BIBF1202 by enzyme(s) expressed in human tissues.

In this study, we aimed to characterize the hydrolysis, glucuronidation, and deglucuronidation reactions of nintedanib in the human liver and intestine, to identify the enzymes responsible for each metabolic step.

DMD Fast Forward. Published on March 16, 2023 as DOI: 10.1124/dmd.122.001113
This article has not been copyedited and formatted. The final version may differ from this version.

Materials and Methods

Materials. Nintedanib, BIBF1202, and BIBF1202-glucuronide (BIBF1202-G) were supplied by Boehringer Ingelheim Pharma GmbH and Co. KG (Ingelheim, Germany). Diisopropyl fluorophosphate (DFP), phenylmethylsulfonyl fluoride (PMSF), 5,5'-dithiobis (2-nitrobenzoic acid) (DTNB), and epigallocatechin 3-gallate (EGCg) were purchased from FUJIFILM Wako Pure Chemical (Osaka, Japan). Bis(*p*-nitrophenyl) phosphate (BNPP), D-saccharic acid 1,4-lactone (SA), uridine 5'-diphosphate-glucuronic acid (UDPGA), alamethicin, and fenofibrate were purchased from Sigma–Aldrich (St. Louis, MO). Fenofibric acid was purchased from Toronto Research Chemicals (Toronto, Canada). Pooled human liver microsomes (HLM) (n = 50), pooled human liver cytosol (HLC) (n = 150), pooled human 9,000 *g* supernatant (S9) (n = 150), and human UGT1A1, UGT1A7, UGT1A8, UGT1A10, UGT2B4, and UGT2B10 Supersomes (recombinant UGTs expressed in baculovirus-infected insect cells) were obtained from Corning (Corning, NY). A mouse anti-human β-glucuronidase antibody (sc-374629) was purchased from Santa Cruz Biotechnology (Santa Cruz, CA). Recombinant human AADAC, CES1, CES2, PON1, PON2, and PON3 were expressed in baculovirus-infected insect cells, and mock transfections were conducted as previously described (Fukami et al., 2010, Watanabe et al., 2010, Hioki et al., 2011). A pooled human plasma sample (n = 68) was purchased from George King Biomedical (Overland Park, KS). All the other chemicals and solvents were of the highest grade commercially available.

Preparation of microsomes from individual human liver samples and *UGT1A1*28* genotyping. Human liver samples from 30 donors (20 Caucasian donors, 5 Hispanic donors, 1 Black donor, and 4 Asian donors) were supplied by the National Disease Research Interchange (Philadelphia, PA) through the Human and Animal Bridging Research Organization (Chiba, Japan). Samples used in each analysis are shown in Supplemental Table 1. The use of human livers was approved by the Ethics Committee of Kanazawa University (Kanazawa, Japan). Microsomal fractions were prepared according to our previous report

DMD Fast Forward. Published on March 16, 2023 as DOI: 10.1124/dmd.122.001113
This article has not been copyedited and formatted. The final version may differ from this version.

(Kobayashi et al., 2012). Human liver homogenates (HLH) were previously prepared (Hashizume et al., 2021). Genomic DNA was extracted from human livers using a Puregene DNA isolation kit (Gentra Systems, Minneapolis, MN) according to the manufacturer's protocols. *UGT1A1*28* genotyping was performed by PCR-single strand conformation polymorphism as described previously (Yamanaka et al., 2005).

Measurement of nintedanib hydrolase activity. Nintedanib hydrolase activity was measured as follows: a typical reaction mixture (final volume of 200 μL) contained 100 mM potassium phosphate buffer (pH 7.4) and enzyme sources (HLM, HLC, HIM, or recombinant human CES1, CES2, and AADAC: 0.04 mg/mL; recombinant human PON1, PON2, or PON3: 0.5 mg/mL; human plasma: 2.5 μL). Upon measuring nintedanib hydrolase activity by PON, 1 mM $CaCl_2$, which is required for PON to exert their activities, was also added. The incubation time and protein concentration were set to be within the linearity for metabolite formation. The reactions were started by adding nintedanib at a final concentration of 20 μM after a 2-min preincubation at 37 °C. Nintedanib was dissolved in 5% acetonitrile, and the final concentration of acetonitrile in the reaction mixture was 0.1%. After a 10-min incubation, the reaction was stopped by adding 100 μL of ice-cold acetonitrile. After the removal of the proteins by centrifugation at 20,400 × g for 5 min, a 50-μL portion of the supernatant was subjected to high-performance liquid chromatography (HPLC), which consisted of an L-7200 autosampler (Hitachi, Tokyo, Japan), an L-7100 pump (Hitachi), an L-7405 UV detector (Hitachi), and a D-2500 Chromato-Integrator (Hitachi). The column used was a Mightysil RP-18 GP (5-μm particle size, 4.6 mm i.d. × 150 mm; Kanto Chemical, Tokyo, Japan). The eluent was monitored at 395 nm with a noise-base clean Uni-3 (Union, Gunma, Japan), which can reduce the noise by the integration of the output and increase the signal by 3-fold by the differentiation of the output and by 5-fold by further amplification with an internal amplifier, resulting in a maximum 15-fold amplification of the signal. The column temperature was set to 35 °C, and the flow rate was 1.0 mL/min. The mobile phases were (A) 100 mM ammonium acetate (pH 8.8) and (B) methanol. The elution conditions were

DMD Fast Forward. Published on March 16, 2023 as DOI: 10.1124/dmd.122.001113
This article has not been copyedited and formatted. The final version may differ from this version.

as follows: 40%–50% B (0–10 min), 50%–95% B (10–15 min), 95% B (15–19 min), 95–40% B (19–20 min), and 40% B (20–22 min). The quantification of BIBF1202 was performed by comparing the HPLC peak area with that of an authentic standard.

Inhibition of nintedanib hydrolase activity. Nintedanib hydrolase activity in HLM was measured in the presence of hydrolase inhibitors or some drugs that may be used in combination with nintedanib. The inhibitors used were PMSF (a general inhibitor of serine hydrolases except for AADAC) (Shimizu et al., 2014), BNPP and DFP (general inhibitors of CESs) (Iwamura et al., 2012), telmisartan (a specific inhibitor of CES2) (Shimizu et al., 2014), and EGCg (a specific inhibitor of AADAC) (Yasuda et al., 2021). Simvastatin, clofibrate, and probucol (antihyperlipidemia drugs), estriol and raloxifene (antiosteoporosis drugs), and enalapril, nifedipine, and carvedilol (antihypertension drugs), which are drugs that may be used in combination with nintedanib, were also used. The final concentration of these inhibitors was set to 100 μM, except for telmisartan and EGCg (50 μM). EGCg was dissolved in distilled water, and the remaining reagents were dissolved in DMSO. The control activities were determined in the presence or absence of 1% DMSO. The activities were measured as described above.

Measurement of fenofibrate hydrolase activity in HLM. Hydrolase activities against fenofibrate, which is a selective CES1 substrate, in individual HLM samples were determined as described in our previous study (Fukami et al., 2015) with slight modifications. The final concentrations of HLM and fenofibrate were 0.05 mg/mL and 5 μM, respectively.

Measurement of BIBF1202 glucuronidation. BIBF1202 glucuronosyltransferase activity was measured as follows: a typical reaction mixture (final volume of 200 μL) contained 30 μM BIBF1202, 100 mM HEPES (pH 6.5), enzyme sources (0.2 mg/mL HLM, HIM, HLH, HLS9, or recombinant human UGT1A1, UGT1A7, UGT1A8, UGT1A10, UGT2B4, and UGT2B10), 10 mM $MgCl_2$, 5 mM UDPGA, and 50 μg/mL alamethicin. The incubation time

DMD Fast Forward. Published on March 16, 2023 as DOI: 10.1124/dmd.122.001113
This article has not been copyedited and formatted. The final version may differ from this version.

and protein concentration were set to be within the linearity for metabolite formation. The reactions were started by adding UDPGA after a 2-min preincubation at 37 °C. BIBF1202 was dissolved in 10 mM HCl, and the final concentration of HCl in the reaction mixture was 100 μM. After a 30-min incubation, the reaction was stopped by adding 100 μL of ice-cold acetonitrile. After the removal of the proteins by centrifugation at 13,000 × g for 20 min, a 50-μL portion of the supernatant was subjected to HPLC. The mobile phases were (A) 100 mM ammonium acetate (pH 4.5) and (B) acetonitrile. The elution conditions were as follows: 5% B (0–0.5 min), 5–20% B (0.5–0.6 min), 20–35% B (0.6–7 min), 35%–90% B (7–9 min), 90% B (9–9.9 min), and 90–5% B (9.9–10 min). The other HPLC conditions were the same as described above. The quantification of BIBF1202-G was performed by comparing the HPLC peak area with that of an authentic standard.

Measurement of BIBF1202-G deglucuronidation. BIBF1202-G deglucuronidation was measured as follows: a typical reaction mixture (final volume of 200 μL) contained 100 mM HEPES (pH 6.5) and enzyme sources (0.2 mg/mL HLM, HIM, or HLS9). The incubation time and protein concentration were set to be within the linearity for metabolite formation. The reactions were started by adding BIBF1202-G after a 2-min preincubation at 37 °C. BIBF1202-G was dissolved in DMSO. The final concentration of DMSO was 1%. After a 60-min incubation, the reaction was stopped by adding 100 μL of ice-cold acetonitrile. After the removal of the proteins by centrifugation at 13,000 × g for 20 min, a 50-μL portion of the supernatant was subjected to HPLC. The conditions for the detection of BIBF1202 were the same as described above. The quantification of BIBF1202 was performed by comparing the HPLC peak area with that of an authentic standard. Because BIBF1202-G is partially hydrolyzed in a nonenzymatic manner, the content of BIBF1202 in the mixture incubated without the enzyme source was subtracted from that with the enzyme source. The fraction of the nonenzymatically formed BIBF1202-G was approximately 15%

DMD Fast Forward. Published on March 16, 2023 as DOI: 10.1124/dmd.122.001113
This article has not been copyedited and formatted. The final version may differ from this version.

Inhibition of BIBF1202-G deglucuronidation. BIBF1202-G deglucuronidation by HLS9 was measured in the presence of SA (a β-glucuronidase inhibitor) (Awolade et al., 2020), DTNB (an ABHD10 and APEH inhibitor) (Iwamura et al., 2012, Suzuki et al., 2010), PMSF and BNPP (ABHD10 inhibitors) (Iwamura et al., 2012), or DFP (an APEH inhibitor) (Suzuki et al., 2010). The control activities were determined in the presence or absence of 1% DMSO. BIBF1202-G deglucuronidation was determined by HPLC as described above.

SDS–PAGE and Western blotting analysis. SDS-polyacrylamide gel electrophoresis (PAGE) and Western blotting analysis were performed to measure β-glucuronidase levels. Individual HLM samples (50 μg) were separated by 10% SDS–PAGE and transferred to polyvinylidene difluoride membranes (Millipore, Billerica, MA). The applied protein amount was within the linear range. After blocking with Odyssey blocking buffer for 1 h, the membranes were incubated with a 1:100 dilution of a mouse anti-human β-glucuronidase antibody for 12 h at room temperature and the corresponding fluorescent dye-conjugated secondary antibody. An Odyssey Infrared Imaging system (LI-COR Biosciences) was used for detection. This analysis was performed in the linear range of band intensity with respect to the protein level.

Kinetic analyses. The substrate concentrations were set as follows: 5 to 100 μM nintedanib and 1 to 200 μM BIBF1202 or BIBF1202-G. The kinetic parameters were calculated based on a curve fitted using a computer program designed for nonlinear regression analysis (GraphPad Prism version 5.0; GraphPad Software, San Diego, CA). The following equations were used:

$$\text{Michaelis–Menten equation: } V = \frac{V_{max} \times [S]}{K_m + [S]}$$

$$CL_{int} = \frac{V_{max}}{K_m}$$

$$\text{Hill equation: } V = \frac{V_{max} \times S^n}{S_{50}^n + S^n}$$

DMD Fast Forward. Published on March 16, 2023 as DOI: 10.1124/dmd.122.001113
This article has not been copyedited and formatted. The final version may differ from this version.

$$CL_{max} = \frac{V_{max}}{\frac{n}{S_{50}}} \times \frac{(n\text{-}1)}{n(n\text{-}1)^{1/n}}$$

where V is the velocity of the reaction, S is the substrate concentration, K_m is the Michaelis–Menten constant, S_{50} is the substrate concentration showing the half-V_{max}, n is the Hill coefficient and V_{max} is the maximum velocity.

Estimation of tissue clearance rates based on *in vitro* data. *In vivo* clearance was estimated using *in vitro* clearance data according to the following equation (Obach et al., 1997; Soars et al., 2002):

$$CL = CL_{int} \times \frac{\text{Microsomal protein}}{\text{Tissue}}\ (\text{mg/g}) \times \frac{\text{Tissue}}{\text{Body weight}}\ (\text{g/kg})$$

where CL_{int} is an *in vitro* clearance value, the microsomal proteins/tissue in the human liver and intestine are 45 and 3 mg/g, respectively, and tissue/body weights in liver and intestine are 20 and 30 g/kg, respectively (Soars et al., 2002).

Correlation analysis between activity and protein expression level in HLM. Relative levels of proteins in microsomal fractions of 25 individual HLM samples were comprehensively evaluated by LC–MS-based untargeted proteomics in our recent study (Kudo et al., in revision). Quantity of each protein was determined from summed abundance of multiple peptides shown in Supplemental Table 2. The enzymes showing a positive correlation among nintedanib hydrolysis, BIBF1202 glucuronidation, or BIBF1202-G deglucuronidation in 25 individual HLM samples were analyzed.

Statistical analyses. The correlation analyses were performed using the Spearman rank method. The significance between two groups was determined by Student's *t*-test. The difference in the BIBF1202 glucuronidations in carriers and noncarrier of *UGT1A1*28* was analyzed by Mann-Whitney *U*-test. A value of $P < 0.05$ was considered statistically significant.

DMD Fast Forward. Published on March 16, 2023 as DOI: 10.1124/dmd.122.001113
This article has not been copyedited and formatted. The final version may differ from this version.

Results

Nintedanib hydrolase activity in human tissue preparations and that of recombinant human hydrolases. Nintedanib hydrolase activities of HLM, HLC, HIM, and plasma were measured at a substrate concentration of 20 μM. As shown in Fig. 1A, the activity of HLM (1.64 ± 0.03 nmol/min/mg protein) was 2.6-fold higher than that of HLC (0.64 ± 0.05 nmol/min/mg protein). BIBF1202 formation was not observed in experiments using HIM and plasma. In the kinetic analysis, the maximum activities of HLM and HLC were observed at 30 μM substrate concentration, and the activities decreased at higher substrate concentrations (Figs. 1B and C). Since the observed enzymatic reaction rate data did not fit the equation describing substrate inhibition enzyme kinetics, the apparent kinetic parameters were estimated using the Michaelis–Menten kinetic equation with activities up to 30 μM substrate concentrations. The K_m values of HLM and HLC were 32.7 ± 5.5 μM and 20.9 ± 1.5 μM, respectively. The V_{max} value of HLM (3.30 ± 0.28 nmol/min/mg protein) was higher than that of HLC (1.24 ± 0.12 nmol/min/mg protein) (Table 1). Thus, it was demonstrated that nintedanib hydrolysis is mainly catalyzed by microsomal enzyme(s) in the liver.

Next, nintedanib hydrolase activities of recombinant CES1, CES2, AADAC, PON1, PON2, and PON3 were measured at a substrate concentration of 20 μM, which was close to the observed K_m values of HLM and HLC. As shown in Fig. 1D, only CES1 showed substantial activity. In the kinetic analysis, the maximum activity of recombinant CES1 was detected at 30 μM substrate concentration, and the activity decreased at higher substrate concentrations. Since the kinetics of CES1 did not fit the equation for substrate inhibition enzyme kinetics, the apparent kinetic parameters were estimated as described above. The K_m value of recombinant human CES1 was 33.5 ± 6.8 μM (Fig. 1E, Table 1), which was close to those of HLM and HLC. Based on these findings, it was suggested that nintedanib is hydrolyzed by CES1 in the liver because CES1 is expressed in the liver but not in the gastrointestinal tract and plasma (Imai, 2006), and CES1 is localized to the endoplasmic reticulum rather than in the cytosol (Fukami et al., 2008).

DMD Fast Forward. Published on March 16, 2023 as DOI: 10.1124/dmd.122.001113
This article has not been copyedited and formatted. The final version may differ from this version.

Inhibition of nintedanib hydrolase activity in HLM. Inhibition experiments using various hydrolase inhibitors were performed to confirm the responsibility of CES1 for nintedanib hydrolysis in the human liver (Fig. 2A). Hydrolysis of nintedanib by HLM was completely inhibited by PMSF, BNPP, and DFP and was potently inhibited by digitonin but not by telmisartan. These results supported that nintedanib hydrolysis is catalyzed by CES1. Interestingly, the activity was significantly increased (2.7-fold) by EGCg.

To examine potential drug–drug interactions, the potencies of 9 drugs that are used to treat hypertension, osteoporosis, or dyslipidemia in inhibiting nintedanib hydrolysis were examined, considering the possibility that they may be used in combination with nintedanib. At concentrations of 100 μM, nifedipine and carvedilol inhibited nintedanib hydrolysis by 80%, and simvastatin, clofibrate, estriol, and raloxifene moderately inhibited nintedanib hydrolysis by 25–60% (Fig. 2B). Nintedanib hydrolysis was not inhibited by probucol or enalapril.

Correlation between hydrolase activities for nintedanib and fenofibrate in a panel of 25 individual HLM samples. To further confirm the role of CES1 in nintedanib hydrolysis, correlation analysis between the hydrolase activities for nintedanib and fenofibrate, which is a specific substrate for CES1, was performed using 25 individual HLM samples. Nintedanib and fenofibrate hydrolysis was not observed in two HLM samples, although substantial protein expression of CES1 was confirmed by Western blotting (data not shown), suggesting that these samples may have loss-of-function mutations in the *CES1* gene. Among the remaining samples, 23-fold and 10-fold interindividual differences in nintedanib and fenofibrate hydrolase activities, respectively, were observed. A significant positive correlation ($r = 0.844$, $P < 0.001$) was observed between these activities (Fig. 3), suggesting the responsibility of CES1 for nintedanib hydrolysis.

DMD Fast Forward. Published on March 16, 2023 as DOI: 10.1124/dmd.122.001113
This article has not been copyedited and formatted. The final version may differ from this version.

Kinetic analyses of BIBF1202 glucuronidation by liver and intestinal microsomes or by recombinant human UGT isoforms (rUGTs). The catalytic activities for BIBF1202 glucuronidation by HLM and HIM were compared. The activities of HLM and HIM fitted to the Hill equation (Figs. 4A, and B, Table 2). HLM and HIM showed similar S_{50} values (33.2 ± 4.5 and 32.0 ± 2.6 μM, respectively), and HLM showed a significantly ($P < 0.001$) higher V_{max} value (118.1 ± 3.4 pmol/min/mg) than HIM (46.9 ± 1.3 pmol/min/mg). By scaling up, the estimated *in vivo* clearance of BIBF1202 glucuronidation in the liver and intestine were 3,291.5 ± 294.1 μL/min/kg body weight and 132.3 ± 5.4 μL/min/kg body weight, respectively, indicating that hepatic glucuronidation could largely contribute to the formation of BIBF1202-G in the body.

UGT1A1, UGT1A3, UGT1A4, UGT1A6, UGT1A9, UGT2B7, UGT2B10, UGT2B15, and UGT2B17 are expressed in various organs, including the liver and intestine (Khatri et al., 2019, Li et al., 2020). UGT2B4 and UGT2B10 are expressed in the liver but not in the intestine, whereas UGT1A7, UGT1A8, and UGT1A10 are expressed in the intestine but not in the liver. UGT1A1, UGT1A7, UGT1A8, and UGT1A10 catalyze the formation of BIBF1202-G, whereas UGT1A3, UGT1A4, UGT1A6, UGT1A9, UGT2B7, and UGT2B15 are not involved in this process (Wind et al., 2019). In this study, we characterized the kinetics of BIBF1202 glucuronidation by UGT1A1, UGT1A7, UGT1A8, and UGT1A10, evaluating whether UGT2B4 and UGT2B10, which were not evaluated in a previous study, actively participate in BIBF1202 glucuronidation. The kinetics of BIBF1202 glucuronidation by rUGT1A1, rUGT1A7, and rUGT1A10 followed the Hill equation, and those of BIBF1202 glucuronidation by rUGT1A8 followed the standard Michaelis–Menten equation (Figs. 4C–F, Table 2). rUGT1A7 had the lowest S_{50} value (21.0 ± 2.4 μM), whereas rUGT1A8 had the highest K_m value (272.8 ± 39.7 μM). rUGT1A1 had a significantly higher V_{max} value (92.6 ± 2.3 pmol/min/mg protein) than rUGT1A7 (3.3 ± 0.3 pmol/min/mg protein), rUGT1A8 (10.3 ± 3.7 pmol/min/mg protein) and rUGT1A10 (15.0 ± 0.6 pmol/min/mg protein), resulting in rUGT1A1 having the highest CL_{int} value (2.5 ± 0.04 μL/min/mg protein, Table 2). rUGT2B4 and rUGT2B10 did not show any activity for BIBF1202 glucuronidation (data not shown).

DMD Fast Forward. Published on March 16, 2023 as DOI: 10.1124/dmd.122.001113
This article has not been copyedited and formatted. The final version may differ from this version.

Considering that UGT1A7, UGT1A8, and UGT1A10 are not expressed in the liver, these results suggested that UGT1A1 mainly catalyzes BIBF1202 glucuronidation in humans.

Effects of the *UGT1A1*28* allele on BIBF1202 glucuronidation. It is well known that the *UGT1A1*28* allele, which harbors an insertion of a dinucleotide (TA) in the $(TA)_6TAA$ element in the *UGT1A1* promoter, results in lower UGT1A1 protein expression (Bosma et al., 1995). The frequencies of the *UGT1A1*28* allele in Asian, African, and Caucasian populations were reported to be 16.0%, 45.7%, and 38.7%, respectively (Burchell et al., 1999). We investigated the impact of *UGT1A1*28* on BIBF1202-G formation using 24 human liver samples, and genotyping was performed on these samples. Of the 24 samples, 7 samples were from noncarriers of the *UGT1A1*28* allele, and 12 and 5 samples were from subjects who were heterozygous and homozygous for the *UGT1A1*28* allele, respectively. As shown in Fig. 5, BIBF1202 glucuronidation in subjects who were homozygous for *UGT1A1*28* (3.45 ± 2.39 pmol/min/mg protein) was significantly ($P < 0.05$) lower than that in noncarriers and subjects who were heterozygous for *UGT1A1*28* (10.85 ± 11.88 pmol/min/mg protein). Thus, it was revealed that mutation in the UGT1A1 promoter region is a critical factor that decreases BIBF1202 glucuronidation.

Deglucuronidation of BIBF1202-G by HLM, HLC, and HLS9. BIBF1202-G is an acyl-glucuronide with a glycosidic ester bond in its chemical structure. We investigated whether BIBF1202-G could be deglucuronidated in the human liver. The deglucuronidation rates of 20 μM BIBF1202-G by HLM (267.6 ± 21.9 pmol/min/mg protein), HLC (341.8 ± 49.1 pmol/min/mg protein), and HLS9 (299.3 ± 19.9 pmol/min/mg protein) were similar (Fig. 6A). According to the kinetic analysis, deglucuronidation by HLS9 linearly increased up to a substrate concentration of 200 μM. The CL_{int} calculated from the initial slope was 10.5 ± 2.0 μL/min/mg protein (Fig. 6B, Table 3), and the value was 70-fold higher than that of BIBF1202 glucuronidation by HLS9 (0.15 ± 0.01 μL/min/mg protein). Given the high CL_{int} of

DMD Fast Forward. Published on March 16, 2023 as DOI: 10.1124/dmd.122.001113
This article has not been copyedited and formatted. The final version may differ from this version.

BIBF1202-G deglucuronidation, the *in vitro* BIBF1202 glucuronidation by HLM or HIM may be underestimated.

Inhibition and correlation analyses to identify the enzyme responsible for the deglucuronidation of BIBF1202-G. To identify the enzyme that catalyzes BIBF1202-G deglucuronidation in the human liver, inhibition analysis using various hydrolase inhibitors was performed. BIBF1202-G deglucuronidation by HLS9 was substantially inhibited by SA but not by DTNB, PMSF, BNPP, or DFP (Fig. 6C), suggesting that β-glucuronidase is responsible for BIBF1202-G deglucuronidation. Human β-glucuronidase is a sole isoform belonging to glycosyl hydrolase family 2 (Henrissat, 1991) and an acid hydrolase (Sperker et al., 1997). We investigated whether BIBF1202-G deglucuronidation was correlated with β-glucuronidase protein levels in human liver samples. Two and one bands were detected at approximately 75 and 60 kDa, respectively (Fig. 6D) by Western blotting using an anti-β-glucuronidase antibody. A similar phenomenon was reported with the data of Gehrmann et al. (1994), who showed the band pattern of recombinant human β-glucuronidase, and data of Sperker et al. (1997), who showed the band pattern of β-glucuronidase in human liver homogenate samples (Sperker et al. 1997), and it was consistent with the fact that molecular weight of β-glucuronidase is 64 or 76–78 kDa (Awolade et al., 2020). Following the report by Sperker et al. (1997), the sum of the intensities of these three bands was considered to be the β-glucuronidase protein level, and these data were subjected to correlation analysis. As shown in Supplemental Fig. 1, we confirmed the positive correlation ($r = 0.90$, $P < 0.001$) between the β-glucuronidase protein levels and the degree of 4-methylumbelliferyl-β- D-glucuronide (4-MUG) deglucuronidation, which is known to be catalyzed by β-glucuronidase (Sperker et al., 1996). The β-glucuronidase protein levels were moderately correlated with BIBF1202-G deglucuronidations ($r = 0.37$, $P = 0.075$) (Fig. 6D). The results suggest that β-glucuronidase may partly be involved in the deglucuronidation of BIBF1202-G.

DMD Fast Forward. Published on March 16, 2023 as DOI: 10.1124/dmd.122.001113
This article has not been copyedited and formatted. The final version may differ from this version.

Proteomic analyses using a panel of 25 individual HLM. Recently, we demonstrated that untargeted proteomics and subsequent correlation analysis with enzyme activity using a panel of human liver samples is a useful approach to identify the responsible enzymes that are involved in processes (Kudo et al., in revision). We applied this approach, by using 25 individual HLM samples, to three metabolic reactions, namely, nintedanib hydrolysis, BIBF1202 glucuronidation, and BIBF1202-G deglucuronidation. Among the 4,457 proteins quantified in untargeted proteomics, 541 and 1,837 proteins were classified by EC classification as hydrolases (EC 3) and transferases (EC 2), respectively. The hydrolase that showed the highest correlation coefficient (r = 0.80) with nintedanib hydrolase activity was CES1 (Table 4, Fig. 7A). The transferase that showed the highest correlation coefficient (r = 0.96) with BIBF1202 glucuronidation was UGT1A1 (Table 4, Fig. 7B). Thus, correlation analyses using proteomics data also revealed that CES1 and UGT1A1 are responsible for nintedanib hydrolysis and BIBF1202 glucuronidation in the human liver, respectively. The hydrolase (EC 3) that showed the highest correlation efficiency (r = 0.70) with BIBF1202-G deglucuronidation was neutrophil elastase (ELANE). Although there are no reports regarding the inhibitory effects of SA on ELANE activity, it has been reported that the degradation of laminin catalyzed by neutrophile elastase in neutrophil fraction was inhibited by 10 μM DFP (Heck et al., 1990). As shown in Fig. 6C, the deglucuronidation of BIBF1202-G was not inhibited by DFP; therefore, the involvement of neutrophil elastase in the deglucuronidation of BIBF1202-G can be denied. Among the top 10 hydrolases, β-glucuronidase is the only enzyme known to be inhibited by SA, to the best of our knowledge. Collectively, β-glucuronidase is a responsible enzyme for BIBF1202-G deglucuronidation, although the involvement of other enzymes cannot be denied. It has been reported that β-glucuronidase forms a homotetramer to exert activity (Matsuura et al., 2011). Therefore, the mild correlation (P = 0.65) would be due to the low efficiency of tetramer formation or the small interindividual differences in the β-glucuronidase expression level.

DMD Fast Forward. Published on March 16, 2023 as DOI: 10.1124/dmd.122.001113
This article has not been copyedited and formatted. The final version may differ from this version.

Discussion

The first goal of our investigation of nintedanib metabolism was to identify the enzyme(s) responsible for nintedanib hydrolysis. We found that CES1 is the responsible enzyme that mediates nintedanib hydrolysis according to studies using recombinant drug-metabolizing hydrolases (Fig. 1), inhibition analyses (Fig. 2), and correlation analyses using individual HLM samples (Fig. 3). The nintedanib hydrolase activity was observed not only in HLM but also in HLC (Fig. 1), which is consistent with our previous report about the hydrolysis of imidapril, a CES1 substrate (Fukami et al., 2008). Interestingly, in the inhibition analysis, nintedanib hydrolase activity was significantly increased by EGCg, which is a potent and specific inhibitor of AADAC (Yasuda et al., 2021). Some drug-metabolizing enzymes, including P450s, were inhibited by EGCg (Muto et al., 2001, Misaka et al., 2013, Satoh et al., 2016), but there are no reports showing the heteroactivation of drug-metabolizing enzymes by EGCg. We previously reported that the hydrolase activity for fenofibrate, a specific substrate for CES1, in HLM was not altered by EGCg (Yasuda et al., 2021); therefore, it is intriguing that the effects of EGCg on CES1 activity vary between substrates.

It has been reported that the average age of onset of IPF is 70.0 ± 9.0 years (Natsuizaka et al., 2014). In addition, the risk of hypertension, osteoporosis, and dyslipidemia increases with age. Considering their possible use in combination with nintedanib, some drugs that are used in the clinical treatment of these diseases were examined at a fixed concentration of 100 μM in order to determine their potential inhibitory effects on nintedanib hydrolase activity. Although our previous report revealed that simvastatin, estriol, and raloxifene strongly inhibited the *p*-nitrophenyl acetate hydrolysis catalyzed by CES1 (Shimizu et al., 2014), these compounds did not potently inhibit nintedanib hydrolase activity in this study (Fig. 2B). The difference could be due to the higher affinity of nintedanib for CES1 (K_m value, 33.5 ± 6.8 μM) than *p*-nitrophenyl acetate (K_m value, 150.8 ± 17.8 μM) (Fukami et al., 2010). The ratio of the area under the curve (AUC) in the presence and absence of inhibitor (AUC_i/AUC), which is calculated by $1 + [I]/K_i$, is frequently used for prediction of *in vivo* drug–drug

DMD Fast Forward. Published on March 16, 2023 as DOI: 10.1124/dmd.122.001113
This article has not been copyedited and formatted. The final version may differ from this version.

interactions, where [I] is the hepatic concentration of inhibitor and Ki is the inhibition constant. The [I] value could be calculated as $I_{inlet,\ u,\ max}$, the maximum value of the unbound concentration at the inlet to the liver, according to Ito et al. (1998), and this results in in 0.34 and 0.18 μM of nifedipine and carvedilol, respectively. The IC_{50} values of nifedipine and carvedilol in nintedanib hydrolysis by HLM were approximately 20 and 30 μM, respectively (data not shown). In general, K_i values are estimated by $IC_{50}/2$ for competitive inhibition, whereas they are estimated by IC_{50} for uncompetitive or non-competitive inhibition (Draper et al., 1997; Niwa et al., 2005). $IC_{50}/2$ values were applied as K_i values because the AUCi/AUC values are higher if smaller K_i values are used. Even though, the AUCi/AUC values were at most 1.03 and 1.01 for nifedipine and carvedilol, respectively; therefore, these drugs are not expected to affect the pharmacokinetics of nintedanib.

According to the scaling-up analysis of *in vitro* clearance, the *in vivo* clearance of BIBF1202 by glucuronidation in the human liver (3,291.5 ± 294.1 μL/min/kg body weight) was much higher than that in the intestine (132.3 ± 5.4 μL/min/kg body weight), indicating that BIBF1202 glucuronidation occurs predominantly in the liver (Table 2). Taken together, the metabolic conversion of nintedanib by hydrolysis and the subsequent glucuronidation predominantly occurred in the liver. It has been reported that BIBF1202 glucuronidation is catalyzed by UGT1A1, UGT1A7, UGT1A8, and UGT1A10 (Wind et al., 2019). Since UGT1A7, UGT1A8, and UGT1A10 are specifically expressed in the gastrointestinal tract (Tukey and Strassburg, 2001, Radominska-Pandya et al., 1998), the contributions of these UGT isoforms to the glucuronidation of BIBF1202 in the human body would be low. BIBF1202 glucuronidation by HLM from subjects who are homozygous for the *UGT1A1*28* allele was significantly lower than that by HLM from noncarriers and subjects who are heterozygous for *UGT1A1*28* (Fig. 6), which is the major reason for the low glucuronidation abilities of UGT1A1 substrates such as bilirubin (Fisher et al., 2000), estradiol (Gagné et al., 2002), and SN-38 (Paoluzzi et al., 2004). Furthermore, BIBF1202 glucuronidation was strongly correlated with UGT1A1 protein level or estradiol glucuronidation (Fig. 7 and

Supplemental Fig. 2). These results suggested that UGT1A1 is a responsible enzyme for glucuronidation of BIBF1202.

Interestingly, we found that in HLS9, the CL_{int} value of BIBF1202-G deglucuronidation was 70-fold higher than that of BIBF1202 glucuronidation (Table 3). Therefore, BIBF1202 glucuronidation by HLM or HIM (Table 2) may be underestimated due to the deglucuronidation of BIBF1202-G. Our laboratory previously revealed that mycophenolic acyl-glucuronide was efficiently deglucuronidated by human α/β hydrolase domain containing 10 (ABHD10), which suppressed the formation of mycophenolic acyl-glucuronide (Iwamura et al., 2012). Suzuki et al. (2010) reported that valproic acid acyl-glucuronide was deglucuronidated by APEH in humans. These authors claimed that the decreased plasma concentration of valproic acid after the coadministration of meropenem in dogs could be due to the inhibition of the APEH-mediated deglucuronidation of valproic acid glucuronide by meropenem (Suzuki et al., 2016). We compared the deglucuronidation of BIBF1202-G by HLM, HLC, and HLS9 to predict the enzyme responsible for the deglucuronidation of BIBF1202-G because the subcellular localization of enzymes known to catalyze the deglucuronidation reaction is different, viz. cytosol for APEH; mitochondria and cytosol for ABHD10; and endoplasmic reticulum and lysosomes for β-glucuronidase (Awolade et al., 2020). According to our experimental data, HLM, HLC, and HLS9 showed similar rates of BIBF1202-G deglucuronidation (Fig. 6A). Therefore, we could not surmise, from these data, the enzyme responsible for BIBF1202-G deglucuronidation. An inhibition study using SA and correlation analysis between β-glucuronidase protein levels and BIBF1202-G deglucuronidation in a panel of 25 individual HLM samples (Figs. 6 and 7) suggested a responsibility of hepatic β-glucuronidase for BIBF1202-G deglucuronidation. This is also corroborated by a significant correlation between BIBF1202-G deglucuronidation and 4-MUG deglucuronidation (Supplemental Fig. 2). The BIBF1202-G deglucuronidation at pH 6.5 was higher than that at pH 7.4 (data not shown), which was partly supported by a previous report that the optimal pH of β-glucuronidase is ~4.5 (Awolade et al., 2020). Nintedanib is mainly eliminated via biliary excretion, resulting in 93.4% recovery in feces within 120 h

after oral administration. Since BIBF1202-G is rarely detected in feces, β-glucuronidase in the gut flora may also catalyze the deglucuronidation of BIBF1202- G.

It is known that acyl-glucuronides can covalently bind to proteins and that such adducts may cause adverse reactions (Bailey et al., 2003). Relating to seminal work by Benet et al. (1993), Sawamura et al. (2010) reported that the half-lives of acyl-glucuronides in potassium phosphate buffer (pH 7.4) can be an index of toxicity; the half-lives of acyl-glucuronides, the parent drugs of which are classified into the "safe" group, were longer than 7.2 hr, whereas those, the parent drugs of which are classified into the "warning" group, were shorter than 3.2 h. It has been reported that the half-life of BIBF1202-G in 0.1 M phosphate buffer (pH 7.4) is 10.5 hr, revealing that BIBF1202-G is relatively stable (Stopfer et al., 2011) and is unlikely to cause toxicity based on potential covalent binding to protein.

In conclusion, we thoroughly characterized the biochemistry and enzymology of the major pathways of nintedanib metabolism in humans. We showed that CES1 is responsible for the hydrolysis of nintedanib, UGT1A1 is responsible for the subsequent glucuronidation, and the formed acyl-glucuronide is efficiently hydrolyzed in the human liver mainly by β-glucuronidase. The findings in this study would be useful to interpret the interindividual differences in the pharmacokinetics of nintedanib.

DMD Fast Forward. Published on March 16, 2023 as DOI: 10.1124/dmd.122.001113
This article has not been copyedited and formatted. The final version may differ from this version.

Data Availability

The proteomics data used in this study are openly available in the ProteomeXchange Consortium (http://www. protemexchange.org/, PXD038055) via the POST partner repository (http://jpostdb.org, JPST001523). All other data presented are contained within the manuscript/supplemental data.

Author contributions

Participated in research design: Nakashima, Sato, Fukami, Nakajima

Conducted experiments: Nakashima, Sato, Kudo, Hashiba, Morinaga

Contributed new reagents or analytical tools: Nakashima, Sato, Kudo, Morinaga, Ludwig-Schwellinger, Matsui, Ishiguro, Ebner

Performed data analysis: Nakashima, Sato, Fukami, Nakano, Kudo, Morinaga, Ludwig-Schwellinger, Matsui, Ishiguro, Ebner, Nakajima

Wrote or contributed to the writing of the manuscript: Nakashima, Sato, Fukami, Nakano, Kudo, Morinaga, Ludwig-Schwellinger, Matsui, Ishiguro, Ebner, Nakajima

DMD Fast Forward. Published on March 16, 2023 as DOI: 10.1124/dmd.122.001113
This article has not been copyedited and formatted. The final version may differ from this version.

References

Azuma A, Taniguchi H, Inoue Y, Kondoh Y, Ogura T, Homma S, Fujimoto T, Sakamoto W, Sugiyama Y, and Nukiwa T. (2016) Nintedanib in Japanese patients with idiopathic pulmonary fibrosis: A subgroup analysis of the INPULSIS® randomized trials. *Respirology* 22: 750-757.

Awolade P, Cele N, Kerru N, Gummidi L, Oluwakemi E, and Singh P (2020) Therapeutic significance of β-glucuronidase activity and its inhibitors: A review. *Eur J Med Chem* 187: 111921.

Bailey MJ and Dickinson RG (2003) Acyl glucuronide reactivity in perspective: biological consequences. *Chem Biol Interact* 145: 117-137.

Benet LZ, Spahn-Langguth H, Iwakawa S, Volland C, Mizuma T, Mayer S, Mutschler E, and Lin ET (1993) Predictability of the covalent binding of acidic drugs in man. *Life Sci* 53: 141-146.

Bosma PJ, Chowdhury JR, Bakker C, Gantla S, de Boer A, Oostra BA, Lindhout D, Tytgat GN, Jansen PL, and Oude Elferink RP, and Chowdhury NR (1995) The genetic basis of the reduced expression of bilirubin UDP-glucuronosyltransferase 1 in Gilbert's syndrome. *N Engl J Med* 333: 1171-1175.

Burchell B, Hume R. Molecular genetic basis of Gilbert's syndrome (1999) *J Gastroenterol Hepatol* 14: 960-966.

Chen KLA, Liu X, Zhao YC, Hieronymi K, Rossi G, Auvil LS, Welge M, Bushell C, Smith RL, Carlson KE, Kim SH, Katzenellenbogen JA, Miller MJ, and Madak-Erdogan Z (2018) Long-term administration of conjugated estrogen and bazedoxifene decreased murine fecal β-glucuronidase activity without impacting overall microbiome community. *Sci Rep* 8: 8166.

Draganov DI, Teiber JF, Speelman A, Osawa Y, Sunahara R, and La Du BN (2005) Human paraoxonases (PON1, PON2, and PON3) are lactonases with overlapping and distinct substrate specificities. *J Lipid Res* 46: 1239-47.

Draper AJ, Madan A, and Parkinson A (1997) Inhibition of coumarin 7-hydroxylase activity in human liver microsomes. *Arch Biochem Biophys* 341: 47-61.

FDA Center for Drug Evaluation and Research (2014) Nintedanib clinical pharmacology NDA review.

Fisher MB, VandenBranden M, Findlay K, Burchell B, Thummel KE, Hall SD, and Wrighton SA (2000) Tissue distribution and interindividual variation in human UDP-glucuronosyltransferase activity: relationship between UGT1A1 promotor genotype and variability in a liver bank. *Pharmacogenetics* 10: 727–739.

Fukami T, Nakajima M, Maruichi T, Takahashi S, Takamiya M, Aoki Y, McLeod HL, and Yokoi T (2008) Structure and characterization of human *carboxylesterase 1A1, 1A2, and 1A3* genes. *Pharmacogenet Genomics* 18: 911-920.

Fukami T, Takahashi S, Nakagawa N, Maruichi T, Nakajima M, and Yokoi T (2010) *In vitro* evaluation of inhibitory effects of antidiabetic and antihyperlipidemic drugs on human carboxylesterase activities. *Drug Metab Dispos* 38: 2173-2178.

Fukami T, Kariya M, Kurokawa T, Iida A, and Nakajima M (2015) Comparison of substrate specificity among human arylacetamide deacetylase and carboxylesterases. *Eur J Pharm Sci* 78:47-53.

Fukami T, Yokoi T, and Nakajima M (2022) Non-P450 drug-metabolizing enzymes: contribution to drug disposition, toxicity, and development. *Annu Rev Pharmacol Toxicol* 62: 405–425.

Gagné JF, Montminy V, Belanger P, Journault K, Gaucher G, and Guillemette C (2002) Common human UGT1A polymorphisms and the altered metabolism of irinotecan active metabolite 7-ethyl-10-hydroxycamptothecin (SN-38). *Mol Pharmacol* 62: 608–617.

Gehrmann MC, Opper M, Sedlacek HH, Bosslet K, and Czech J (1994) Biochemical properties of recombinant human β-glucuronidase synthesized in baby hamster kidney cells. *Biochem J* 301: 821-828.

Hashizume H, Fukami T, Mishima K, Arakawa H, Mishiro K, Zhang Y, Nakano M, and Nakajima M (2021) Identification of an isoform catalyzing the CoA conjugation of nonsteroidal anti-inflammatory drugs and the evaluation of the expression levels of acyl-CoA synthetases in the human liver. *Biochem Pharmacol* 183: 114303.

Heck LW, Blackburn WD, Irwin MH, and Abrahamson DR (1990) Degradation of basement membrane laminin by human neutrophil elastase and cathepsin G. *Am J Pathol* 136: 1267-1274.

Henrissat B (1991) A classification of glycosyl hydrolases based on amino acid sequence similarities. *Biochem J* 280: 309-316.

Hioki T, Fukami T, Nakajima M, and Yokoi T (2011) Human paraoxonase 1 is the enzyme responsible for pilocarpine hydrolysis. *Drug Metab Dispos* 39: 1345-1352.

Imai T (2006) Human carboxylesterase isozymes: catalytic properties and rational drug design. *Drug Metab Pharmacokinet* 21: 173–185.

Ito K, Iwatsubo T, Kanamitsu S, Ueda K, Suzuki H, and Sugiyama Y (1998) Prediction of pharmacokinetic alterations caused by drug-drug interactions: metabolic interaction in the liver. *Pharmacol Rev*. 50: 387-412.

Iwamura A, Fukami T, Higuchi R, Nakajima M, and Yokoi T (2012) Human α/β hydrolase domain containing 10 (ABHD10) is responsible enzyme for deglucuronidation of mycophenolic acid acyl-glucuronide in liver. *J Biol Chem* 287: 9240-9249.

Khatri R, Fallon JK, Rementer RJB, Kulick NT, Lee CR, and Smith PC (2019) Targeted quantitative proteomic analysis of drug metabolizing enzymes and transporters by nano LC-MS/MS in the sandwich cultured human hepatocyte model. *J Pharmacol Toxicol Methods* 98:106590.

Kobayashi Y, Fukami T, Nakajima A, Watanabe A, Nakajima M, and Yokoi T (2012) Species differences in tissue distribution and enzyme activities of arylacetamide deacetylase in human, rat, and mouse. *Drug Metab Dispos*. 40:671-9.

Li J, and Zhu HJ (2020) Liquid chromatography-tandem mass spectrometry (LC-MS/MS)-based proteomics of drug-metabolizing enzymes and transporters. *Molecules* 25: 2718.

Matsuura T, Hosoda K, Ichihashi N, Kazuta Y, and Yomo T (2011) Kinetic analysis of β-galactosidase and β-glucuronidase tetramerization coupled with protein translation. *J Biol Chem* 286: 22028–22034.

Misaka S, Kawabe K, Onoue S, Werba JP, Giroli M, Tamaki S, Kan T, Kimura J, Watanabe H, and Yamada S (2013) Effects of green tea catechins on cytochrome P450 2B6, 2C8, 2C19, 2D6 and 3A activities in human liver and intestinal microsomes. *Drug Metab Pharmacokinet* 28: 244-249.

Muto S, Fujita K, Yamazaki Y, and Kamataki T (2001) Inhibition by green tea catechins of metabolic activation of procarcinogens by human cytochrome P450. *Mutat Res* 479: 197-206.

Natsuizaka M, Chiba H, Kuronuma K, Otsuka M, Kudo K, Mori M, Bando M, Sugiyama Y, and Takahashi H (2014) Epidemiologic survey of Japanese patients with idiopathic pulmonary fibrosis and investigation of ethnic differences. *Am J Respir Crit Care Med* 190: 773-779.

Niwa T, Shiraga T, and Takagi A (2005) Effect of antifungal drugs on cytochrome P450 (CYP) 2C9, CYP2C19, and CYP3A4 activities in human liver microsomes. *Biol Pharm Bull* 28: 1805–1808.

Obach RS (1997) Nonspecific binding to microsomes: impact on scale-up of in vitro intrinsic clearance to hepatic clearance as assessed through examination of warfarin, imipramine, and propranolol. *Drug Metab Dispos* 25: 1359-1369.

Paoluzzi L, Singh AS, Price DK, Danesi R, Mathijssen RH, Verweij J, Figg WD, and Sparreboom A (2004) Influence of genetic variants in UGT1A1 and UGT1A9 on the in vivo glucuronidation of SN-38. *J Clin Pharmacol* 44: 854-860.

Radominska-Pandya A, Little JM, Pandya JT, Tephly TR, King CD, Barone GW, and Raufman JP (1998) UDP-glucuronosyltransferases in human intestinal mucosa. *Biochim Biophys Acta* 1394: 199-208.

Raghu G, Rochwerg B, Zhang Y, Garcia CA, Azuma A, Behr J, Brozek JL, Collard HR, Cunningham W, Homma S, Johkoh T, Martinez FJ, Myers J, Protzko SL, Richeldi L, Rind D, Selman M, Theodore A, Wells AU, Hoogsteden H, and Schünemann HJ; American Thoracic Society; European Respiratory society; Japanese Respiratory Society; and Latin American Thoracic Association. An official ATS/ERS/JRS/ALAT clinical practice guideline: treatment of idiopathic pulmonary fibrosis. An Update of the 2011 Clinical Practice Guideline (2015) *Am J Respir Crit Care Med* 192: e3-e19.

Richeldi L, Collard HR, and Jones MG (2017) Idiopathic pulmonary fibrosis. *Lancet* 389: 1941-1952.

Satoh T, Fujisawa H, Nakamura A, Takahashi N, and Watanabe K (2016) Inhibitory effects of eight green tea catechins on cytochrome P450. *J Pharm Pharm Sci*; 19: 188-197.

Sawamura R, Okudaira N, Watanabe K, Murai T, Kobayashi Y, Tachibana M, Ohnuki T, Masuda K, Honma H, Kurihara A, and Okazaki O (2010) Predictability of idiosyncratic drug toxicity risk for carboxylic acid-containing drugs based on the chemical stability of acyl glucuronide. *Drug Metab Dispos*. 38: 1857-64.

Shimizu M, Fukami T, Nakajima M, and Yokoi T (2014) Screening of specific inhibitors for human carboxylesterases or arylacetamide deacetylase. *Drug Metab Dispos* 42: 1103-1109.

Soars MG, Burchell B, and Riley RJ (2002) In vitro analysis of human drug glucuronidation and prediction of in vivo metabolic clearance. *J Pharmacol Exp Ther* 301:382-90.

Sperker B, Mürdter TE, Schick M, Eckhardt K, Bosslet K, and Kroemer HK (1997) Interindividual variability in expression and activity of human β-glucuronidase in liver and kidney: consequences for drug metabolism. *J Pharmacol Exp Ther* 281: 914-920.

Sperker B, Schick M, and Kroemer HK (1996) High-performance liquid chromatographic quantification of 4-methylumbelliferyl-β-D-glucuronide as a probe for human β-

glucuronidase activity in tissue homogenates. *J Chromatogr B Biomed Appl* 685: 181-184.

Stopfer P, Rathgen K, Bischoff D, Lüdtke S, Marzin K, Kaiser R, Wagner K, and Ebner T (2011) Pharmacokinetics and metabolism of BIBF 1120 after oral dosing to healthy male volunteers. *Xenobiotica* 41: 297-311.

Suzuki E, Yamamura N, Ogura Y, Nakai D, Kubota K, Kobayashi N, Miura S, and Okazaki O (2010) Identification of valproic acid glucuronide hydrolase as a key enzyme for the interaction of valproic acid with carbapenem antibiotics. *Drug Metab Dispos* 38: 1538-1544.

Suzuki E, Nakai D, Ikenaga H, Fusegawa K, Goda R, Kobayashi N, Kuga H, and Izumi T (2016) In vivo inhibition of acylpeptide hydrolase by carbapenem antibiotics causes the decrease of plasma concentration of valproic acid in dogs. *Xenobiotica*. 46: 126-131.

Tukey RH, Strassburg CP (2001) Genetic multiplicity of the human UDP-glucuronosyltransferases and regulation in the gastrointestinal tract. *Mol Pharmacol* 59: 405-414.

Watanabe A, Fukami T, Takahashi S, Kobayashi Y, Nakagawa N, Nakajima M, and Yokoi T (2010) Arylacetamide deacetylase is a determinant enzyme for the difference in hydrolase activities of phenacetin and acetaminophen. *Drug Metab Dispos* 38: 1532-1537.

Wind S, Schmid U, Freiwald M, Marzin K, Lotz R, Ebner T, Stopfer P, and Dallinger C (2019) Clinical pharmacokinetics and pharmacodynamics of nintedanib. *Clin Pharmacokinet* 58: 1131-1147.

Yamanaka H, Nakajima M, Hara Y, Katoh M, Tachibana O, Yamashita J and Yokoi T (2005) Urinary excretion of phenytoin metabolites, 5-(4'-hydroxyphenyl)-5-phenylhydantoin and its *O*-glucuronide in human and analysis of genetic polymorphisms of UDP-glucuronosyltransferases. *Drug Metab Pharmacokinet* **20**:135-43.

Yasuda K, Watanabe K, Fukami T, Nakashima S, Ikushiro SI, Nakajima M, and Sakaki T (2021) Epicatechin gallate and epigallocatechin gallate are potent inhibitors of human arylacetamide deacetylase. *Drug Metab Pharmacokinet* 39:100397.

DMD Fast Forward. Published on March 16, 2023 as DOI: 10.1124/dmd.122.001113
This article has not been copyedited and formatted. The final version may differ from this version.

Footnotes

The authors declare no conflict of interest and this work received no external funding.

Send reprint requests to: Miki Nakajima, Ph.D. Faculty of Pharmaceutical Sciences, Kanazawa University, Kakuma-machi, Kanazawa 920-1192, Japan. E-mail: nmiki@p.kanazawa-u.ac.jp

DMD Fast Forward. Published on March 16, 2023 as DOI: 10.1124/dmd.122.001113
This article has not been copyedited and formatted. The final version may differ from this version.

Figure legends

Fig. 1. Nintedanib hydrolase activities by human tissues and recombinant human hydrolases. (A) Nintedanib hydrolase activities by human liver or intestine preparations (0.04 mg/mL) and plasma (10 μL/mL) were measured at 20 μM substrate concentration. (B, C) Kinetic analyses of nintedanib hydrolase activity by (B) HLM and (C) HLC were performed at a range of 5 to 100 μM of nintedanib. (D) Nintedanib hydrolase activity by recombinant human hydrolases (0.04 mg/mL) was measured at 20 μM substrate concentration. (E) Kinetic analysis of nintedanib hydrolase activity by recombinant CES1 was performed at a range of 5 to 100 μM of nintedanib. Each column and point represent the mean ± SD of triplicate determinations. ND: Not detectable.

Fig. 2. Inhibitory effects of hydrolase inhibitors and clinically used drugs on nintedanib hydrolase activity in HLM. Inhibitory effects of some hydrolase inhibitors (A) or clinically used drugs (B) on nintedanib hydrolase activity were evaluated at 20 μM substrate concentration. The final concentration of inhibitors was set to be 100 μM, except for telmisartan and EGCg (50 μM). Each column represents the mean ± SD of triplicate determinations. ND: Not detectable.

Fig. 3. Correlation analysis between nintedanib and fenofibrate hydrolase activities in a panel of 24 individual HLM samples. Nintedanib hydrolase activity was measured at 20 μM nintedanib. Fenofibrate hydrolase activity was measured at 5 μM fenofibrate. Each point represents the mean of duplicate determinations.

Fig. 4. Kinetic analyses for BIBF1202 glucuronidation by human liver or intestine microsomes and recombinant human UGT isoforms. The activities were measured using (A) pooled HLM, (B) pooled HIM, (C) recombinant UGT1A1, (D) UGT1A7, (E) UGT1A8, and

(F) UGT1A10 at a range of 5 to 200 μM of BIBF1202. Each point represents the mean ± SD of triplicate determinations.

Fig. 5. Effects of the *UGT1A1*28* allele on BIBF1202 glucuronidation by HLM. The BIBF1202-G deglucuronidation was determined at 30 μM substrate concentration. Each point represents the mean of duplicate determinations. The difference in the BIBF1202 glucuronidations between carriers and noncarrier of *UGT1A1*28* was analyzed by Mann-Whitney *U*-test. $^{*}P < 0.05$.

Fig. 6. Involvement of β-glucuronidase in BIBF1202-G deglucuronidation in the human liver. (A) BIBF1202-G deglucuronidation by pooled HLM, HLC, and HLS9 was measured at 20 μM substrate concentration. (B) Kinetic analyses of BIBF1202-G deglucuronidation by pooled HLS9 was performed at a range of 5 to 200 μM of BIBF1202-G. (C) Inhibitory effects of various inhibitors of hydrolases on BIBF1202-G deglucuronidation by HLS9. Each column or point represents the mean ± SD of triplicate determinations. $^{***}P < 0.001$ compared with control. (D) Correlation analysis between BIBF1202-G deglucuronidation and β-glucuronidase protein levels in a panel of 24 individual HLM samples. The BIBF1202-G deglucuronidation was determined at 20 μM substrate concentration. β-Glucuronidase protein levels determined by Western blotting are represented as relative levels to the sample with the lowest expression level. Each point represents the mean of duplicate determinations.

Fig. 7. Correlation analyses between relative protein levels determined by untargeted proteomics and enzyme activities in a panel of 25 individual HLM samples. The protein levels of (A) CES1, (B) UGT1A1 or (C) β-glucuronidase determined by untargeted proteomics are represented as relative levels to the sample with the lowest expression levels. The peptide sequences used to quantify CES1, UGT1A1 and β-glucuronidase are shown in Supplemental Table 2. Nintedanib hydrolase activity, BIBF1202 glucuronidation, and

DMD Fast Forward. Published on March 16, 2023 as DOI: 10.1124/dmd.122.001113
This article has not been copyedited and formatted. The final version may differ from this version.

BIBF1202-G deglucuronidation were measured at 20 μM, 30 μM, and 20 μM substrate concentrations, respectively.

DMD Fast Forward. Published on March 16, 2023 as DOI: 10.1124/dmd.122.001113
This article has not been copyedited and formatted. The final version may differ from this version.

Table 1. Kinetic parameters of nintedanib hydrolysis by HLM, HLC, and recombinant CES1.

Enzyme	*K*m	*V*max	CL_{int}
	μM	nmol/min/mg	μL/min/mg
HLM	32.7 ± 5.5	3.30 ± 0.28	102.8 ± 18.9
HLC	20.9 ± 1.5	1.24 ± 0.12	59.3 ± 2.6
Recombinant CES1	33.5 ± 6.8	1.67 ± 0.28	49.9 ± 1.8

DMD Fast Forward. Published on March 16, 2023 as DOI: 10.1124/dmd.122.001113
This article has not been copyedited and formatted. The final version may differ from this version.

Table 2. Kinetic parameters of BIBF1202 glucuronidation by HLM, HIM, rUGT1A1, rUGT1A7, rUGT1A8, or rUGT1A10.

Enzyme	*K*m or S_{50}	n	*V*max	CL_{int}
	μM		pmol/min/mg	μL/min/mg
HLM	33.2 ± 4.5	2.19	118.1 ± 3.4	3.6 ± 0.3*
HIM	32.0 ± 2.6	2.02	46.9 ± 1.3	1.5 ± 0.06
rUGT1A1	37.6 ± 0.07	2.12	92.6 ± 2.3	2.5 ± 0.04
rUGT1A7	21.0 ± 2.4	1.89	3.3 ± 0.3	0.2 ± 0.02
rUGT1A8	272.8 ± 39.7	-	10.3 ± 3.7	0.04 ± 0.003
rUGT1A10	34.7 ± 1.9	1.98	15.0 ± 0.6	0.4 ± 0.002

*$P < 0.001$, kinetic parameters by HLM were compared with those by HIM by Student's *t*-test.

DMD Fast Forward. Published on March 16, 2023 as DOI: 10.1124/dmd.122.001113
This article has not been copyedited and formatted. The final version may differ from this version.

Table 3. Kinetic parameters of BIBF1202 glucuronidation and deglucuronidation by HLS9**.**

Reaction	*K*m	*V*max	CL_{int}
	μM	pmol/min/mg	μL/min/mg
Glucuronidation	32.4 ± 3.4	4.8 ± 0.2	0.15 ± 0.01
Deglucuronidation[a]	NA	NA	10.5 ± 2.0

[a]K_m and V_{max} values were not calculated. CL_{int} was calculated with the initial slope of the velocity versus substrate concentration. NA: Not applicable.

DMD Fast Forward. Published on March 16, 2023 as DOI: 10.1124/dmd.122.001113
This article has not been copyedited and formatted. The final version may differ from this version.

Table 4. Candidate responsible enzyme for nintedanib hydrolysis, BIBF1202-glucuronidation or BIBF1202-G deglucuronidation

RANK	Gene name	Protein name	R
Nintednaib hydrolysis		EC classification: Hydrolase (521)	
1	CES1	Liver carboxylesterase 1	0.73
2	GANAB	Neutral alpha-glucosidase AB	0.69
3	GGT7	Glutathione hydrolase 7	0.68
4	F2	Prothrombin	0.67
5	ENTPD5	Ectonucleoside triphosphate diphosphohydrolase 5	0.67
6	PON1	Serum paraoxonase/arylesterase 1	0.67
7	PLA2G4C	Cytosolic phospholipase A2 gamma	0.66
8	INPP5K	Inositol polyphosphate 5-phosphatase K	0.66
9	MANBA	Beta-mannosidase	0.65
10	PON3	Serum paraoxonase/lactonase 3	0.63
BIBF1202 glucuronidation		EC classification: Transferase (1837)	
1	UGT1A1	UDP-glucuronosyltransferase 1-1	0.97
2	RNF139	E3 ubiquitin-protein ligase RNF139	0.82
3	UGT1A6	UDP-glucuronosyltransferase 1-6	0.8
4	UGT2B4	UDP-glucuronosyltransferase 2B4	0.76
5	DPY19L1	Probable C-mannosyltransferase DPY19L1	0.75
6	CHST7	Carbohydrate sulfotransferase 7	0.74
7	POGLUT2	Protein *O*-glucosyltransferase 2	0.73
8	METTL7A	Methyltransferase-like protein 7A	0.73
9	UGGT1	UDP-glucose:glycoprotein glucosyltransferase 1	0.73
10	UGT1A9	UDP-glucuronosyltransferase 1-9	0.7
BIBF1202-G deglucuronidation		EC classification: Hydrolase (521)	
1	ELANE	Neutrophil elastase	0.70
2	POLD1	DNA polymerase delta catalytic subunit	0.69
3	SCPEP1	Retinoid-inducible serine carboxypeptidase	0.67
4	LACTB2	Endoribonuclease LACTB2	0.66
5	GUSB	β-glucuronidase	0.65
6	MTMR1	Myotubularin-related protein 1	0.63
7	NAGLU	Alpha-*N*-acetylglucosaminidase	0.59
8	GLB1	β-galactosidase	0.54
9	PSMB6	Proteasome subunit beta type-6	0.52
10	MMP8	Neutrophil collagenase	0.50

Fig. 1

DMD Fast Forward. Published on March 16, 2023 as DOI: 10.1124/dmd.122.001113

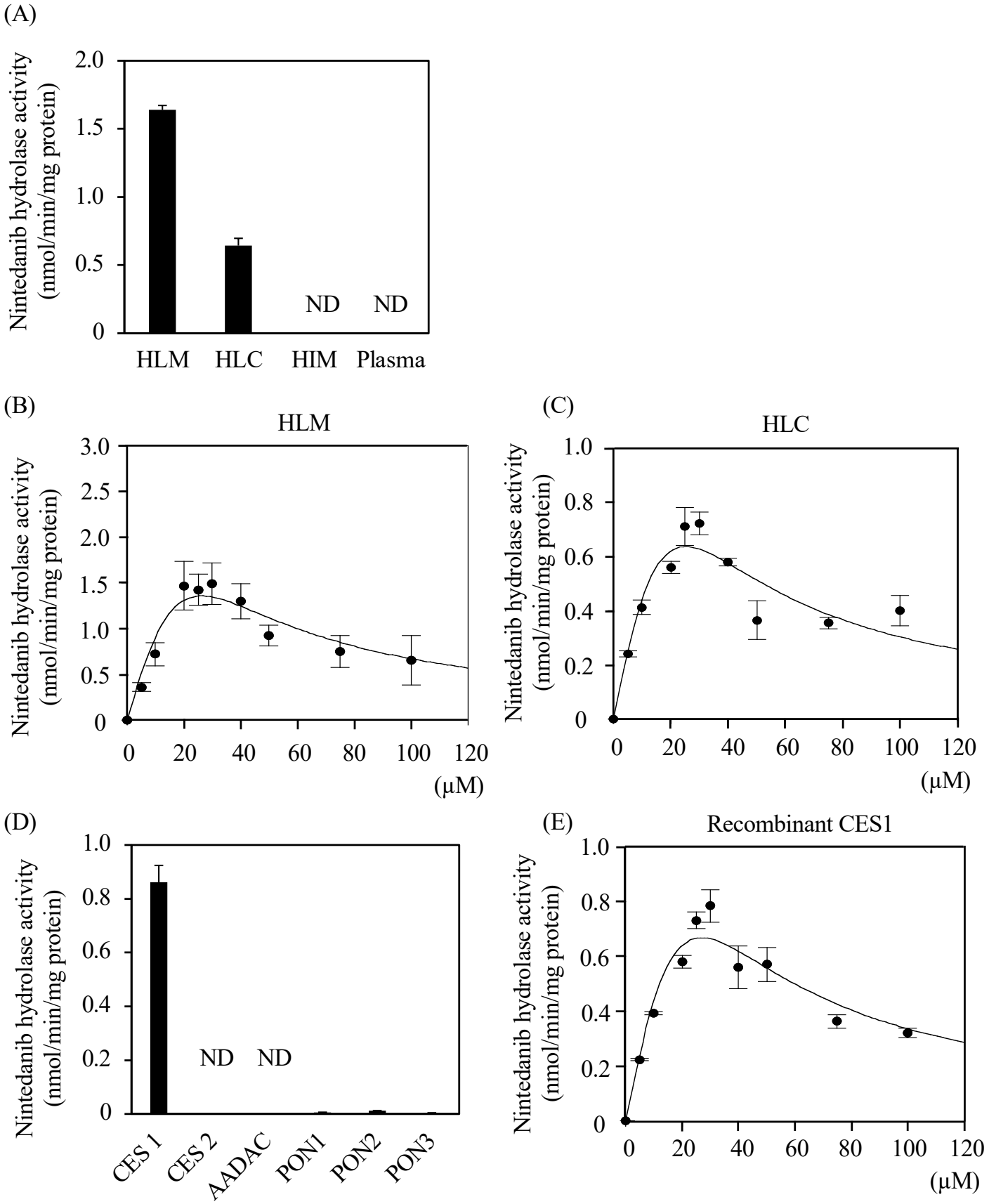

DMD Fast Forward. Published on March 16, 2023 as DOI: 10.1124/dmd.122.001113
This article has not been copyedited and formatted. The final version may differ from this version.

Fig. 2

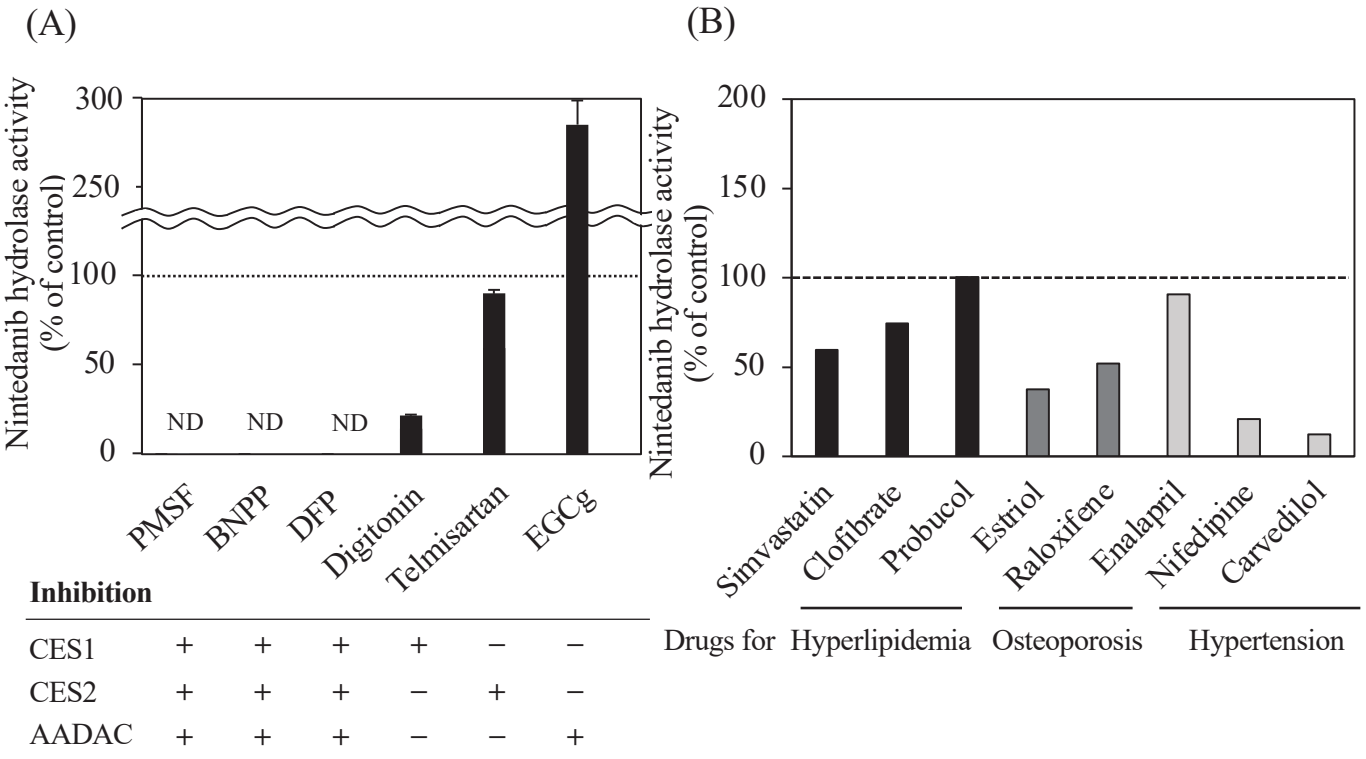

DMD Fast Forward. Published on March 16, 2023 as DOI: 10.1124/dmd.122.001113
This article has not been copyedited and formatted. The final version may differ from this version.

Fig. 3

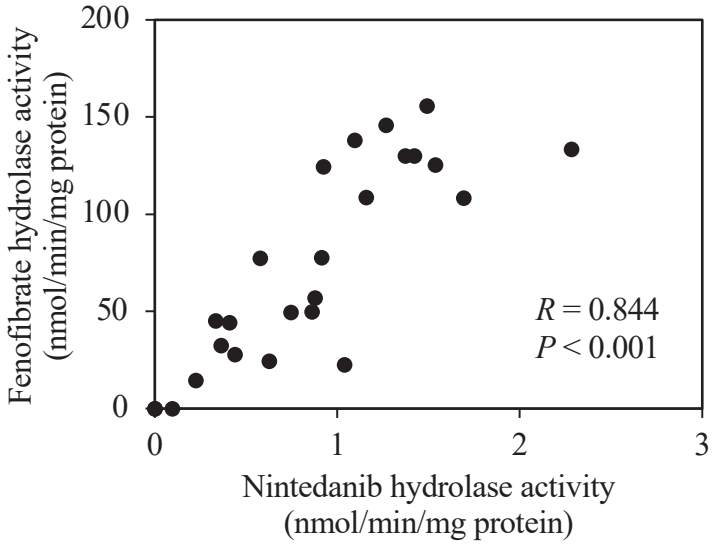

DMD Fast Forward. Published on March 16, 2023 as DOI: 10.1124/dmd.122.001113
This article has not been copyedited and formatted. The final version may differ from this version.

Fig. 4

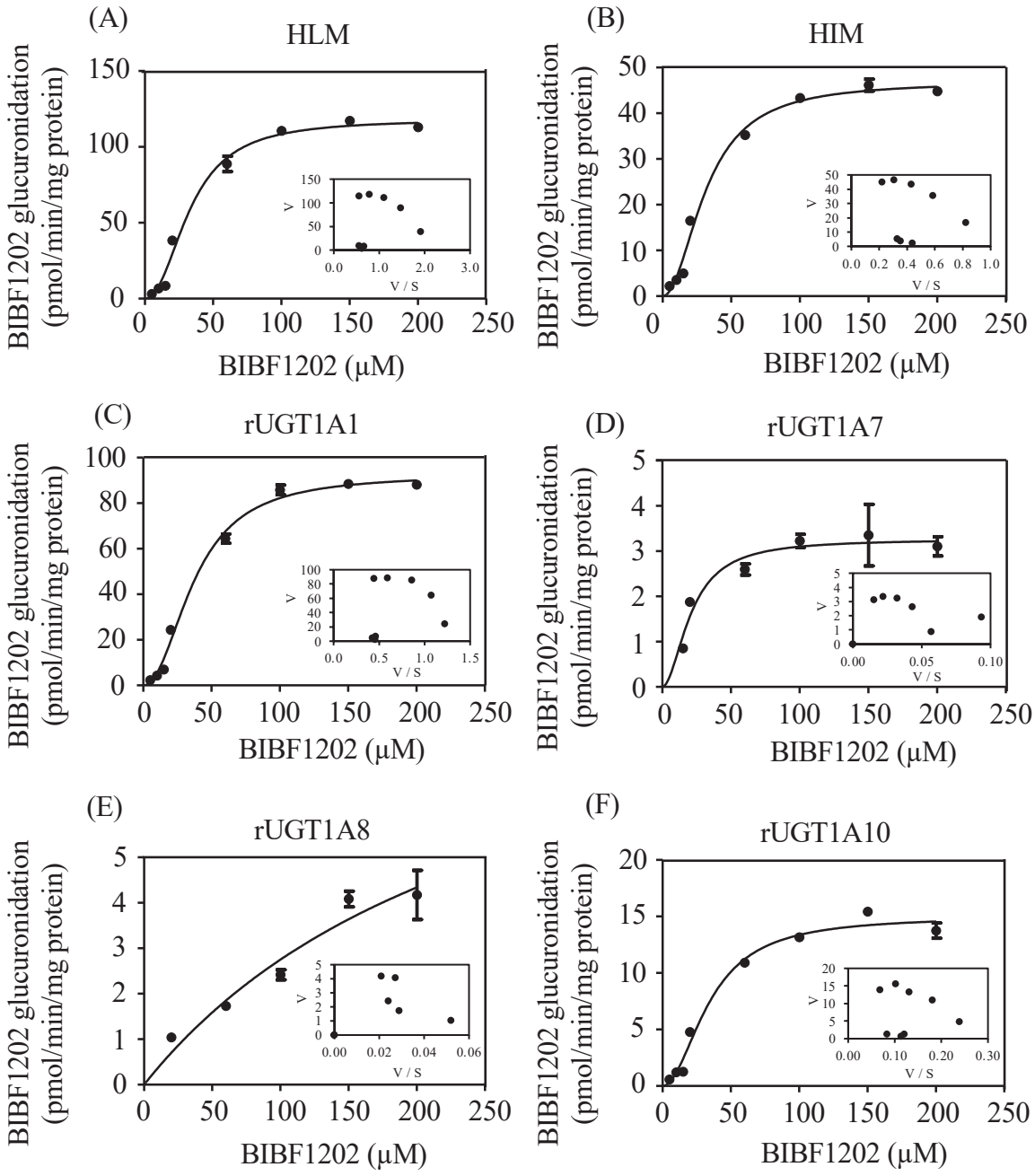

DMD Fast Forward. Published on March 16, 2023 as DOI: 10.1124/dmd.122.001113
This article has not been copyedited and formatted. The final version may differ from this version.

Fig. 5

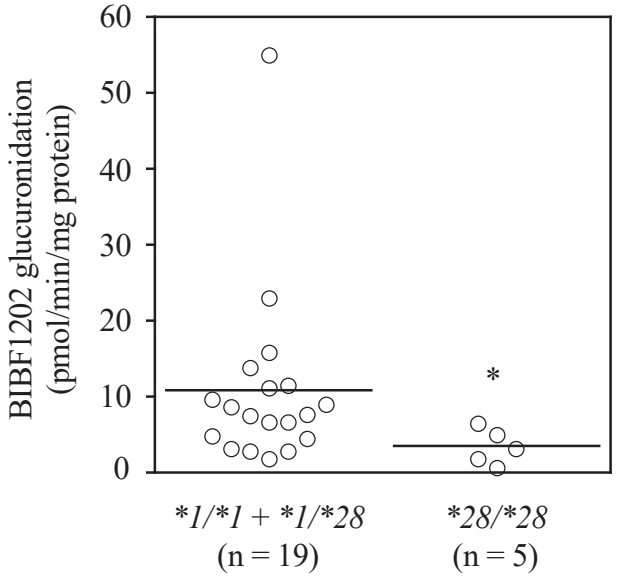

DMD Fast Forward. Published on March 16, 2023 as DOI: 10.1124/dmd.122.001113
This article has not been copyedited and formatted. The final version may differ from this version.

Fig. 6

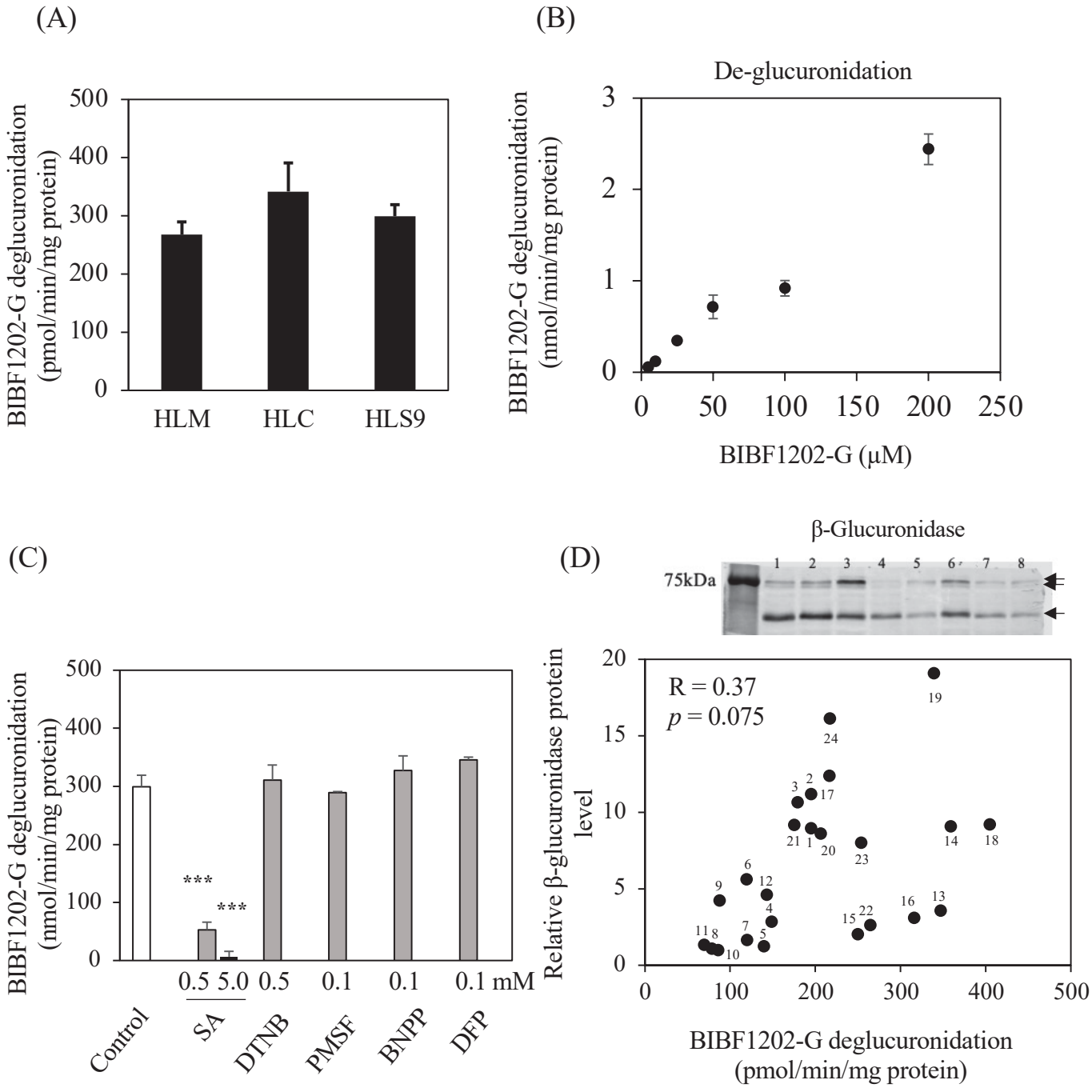

DMD Fast Forward. Published on March 16, 2023 as DOI: 10.1124/dmd.122.001113
This article has not been copyedited and formatted. The final version may differ from this version.

Fig. 7